Bulletin of Engineering Geology and the Environment (2021) 80:2307–2321
https://doi.org/10.1007/s10064-020-02049-6

ORIGINAL PAPER

Experimental study on mechanical properties and failure behaviour of the pre-cracked coal-rock combination

Jiangwei Liu[1] · Na Wu[2] · Guangyao Si[3] · Mingxin Zhao[4]

Received: 22 February 2020 / Accepted: 19 November 2020 / Published online: 26 November 2020

Abstract

The mechanical property of roof is critically important for underground coal mining activities. The existence of hard roof that cannot cave naturally after coal extraction results in an unconsolidated goaf with large voids, and the sudden failure of this type of roof in uncontrolled manner will cause server windblast or rockburst hazard. To address this hazard, pre-existing fractures are created in roof by hydraulic fracturing or blasting to weaken the hard roof and promote its natural caving. The effectiveness of these roof weakening techniques is highly dependent on the geometry of pre-conditioned fractures and its impact on the mechanical behaviour of combined roof-coal strata, which has not been well-explored yet. Therefore, 21 groups of uniaxial compression testing on combined rock-coal specimens with pre-existing cracks were carried out, and the effect of fracture length and angle on the mechanical properties and failure modes of combined rock-coal strata were investigated. It can be concluded that longer cracks and/or cracks with angle closer to 30° tend to have the following characteristics. (1) The more gentle the stress-strain curve of the combined coal and rock tends to be, the larger the decrease range of its elastic modulus, peak strength and peak strain, and the smaller the strain interval corresponding to the elastic-plastic stage. The results show that the artificial fracture weakens the mechanical properties of composite coal and accelerates the process from micro-crack to macro failure. (2) When the specimen enters the plastic stage, the acoustic emission jumps sharply; the cumulative number of micro-cracks and the cumulative energy released during the whole loading process gradually decrease, and the number of micro-cracks and the released energy at the moment of failure also decrease gradually. (3) The crack-initiating stress for combined coal-rock specimens gradually decreases via one of three typical modes: preferential crack initiation of coal, simultaneous crack initiation of combined coal-rock and preferential crack initiation of rock, which also matches with coal failure, rock-coal failure and rock failure in the combined specimens. Thus, to promote the continuous fracture of the roof under loading, the length and orientation of the pre-conditioned cracks must be controlled and optimised.

Keywords Combined coal-rock · Pre-existing fractures · Failure mode · Crack angle · Crack length

Introduction

Thirty-eight percent of the world's electricity and 71% of the world's steel are produced by coal. Longwall mining as the most productive underground coal extraction method requires the continuous caving of roof strata behind a working face to develop a caved area, which is named as goaf. However, coal seams sometimes may be overlying by strong and hard roofs that cannot cave naturally after coal extraction to develop the goaf. In this case, the hard hanging roof may form a large void area behind the face, and once it fails in an uncontrolled manner, it can result in windblast, rockburst (Kaiser 2012; Mazaira and Konicek 2015; Qiu et al. 2014; Cai et al. 2016; Wu et al. 2020) or outburst (Lin et al. 2015; Si et al. 2015), which is a server threat to coal mine health and safety. To address this hazard, fractures are normally created

✉ Na Wu
wuna0306@mail.dlut.edu.cn

[1] College of Energy and Mining Engineering, Shandong University of Science and Technology, Qingdao 266590, China

[2] State Key Laboratory of Coastal and Offshore Engineering, Dalian University of Technology, Dalian 116024, China

[3] School of Minerals and Energy Resources Engineering, University of New South Wales, Sydney, NSW 2052, Australia

[4] College of Marine Geosciences, Ocean University of China, Qingdao 266590, China

(a) Coal and rock parts to form the combined specimen

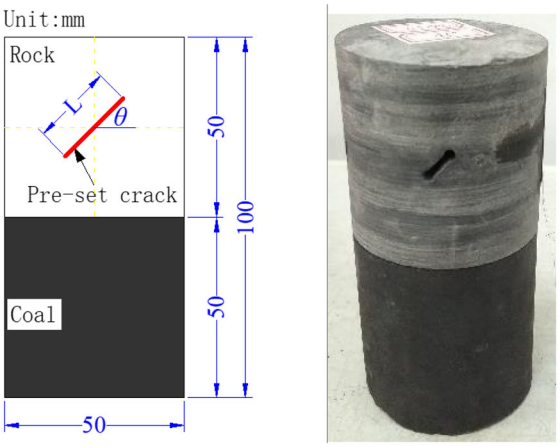

(b) Water-jet cutting to create preconditioned cracks in the combined coal-rock specimen

(c) An overview of all combined specimens with preconditioned cracks in roof rock

Fig. 1 Preparation of combined coal-rock specimens with pre-conditioned cracks. **a** Coal-rock parts to form the combined specimen. **b** Water-jet cutting to create pre-conditioned cracks in the combined coal-rock specimen. **c** An overview of all combined specimens with pre-conditioned cracks in roof rock

in hard roofs by hydraulic fracturing (Huang et al. 2015), water-jet slotting (Si et al. 2015) or blasting (Yang et al. 2016) to weaken the strength of the hard roofs and promote its natural caving. The underpinning knowledge to determine the effectiveness of these techniques is the interactive behaviour of pre-conditioned fractures in the combined roof and coal strata, such as the weakening of mechanical properties, induced seismic response and the damage characteristics of the hard roof after fracturing treatment (Huang et al. 2018; Lu et al. 2015; Tan et al. 2015).

The most common method applied in coal mine to fracture hard roof is based on hydraulic fracturing. High-pressure water is normally injected into the hard roof through boreholes ahead of a working face, which can initiate a connected fracture network, release elastic strain energy and contribute to the roof nature caving (Ouyang 2012; Lin et al. 2011). The development of roof fractures is mainly controlled by the interaction between in situ stress and the natural fracture network. Additionally, different patterns can lead to various weakening degrees of the roof rock and coal strata. In practice, the roof and coal seam are loaded simultaneously, and the deformation of roof fracture can also be affected by the underlying coal seam. Lack of understanding on roof fracture development may result in dynamic disasters such as rock/coal burst or gas outbursts caused by the instability of the combined coal-rock system (Lu et al. 2015; Zhao et al. 2016; Wang et al. 2019; Qiu et al. 2020). Therefore, improving the understanding on the failure in the combined coal-rock strata can provide significant guidance for hydraulic fracturing design to precondition hard roofs, which can reduce the risk of dynamic hazards.

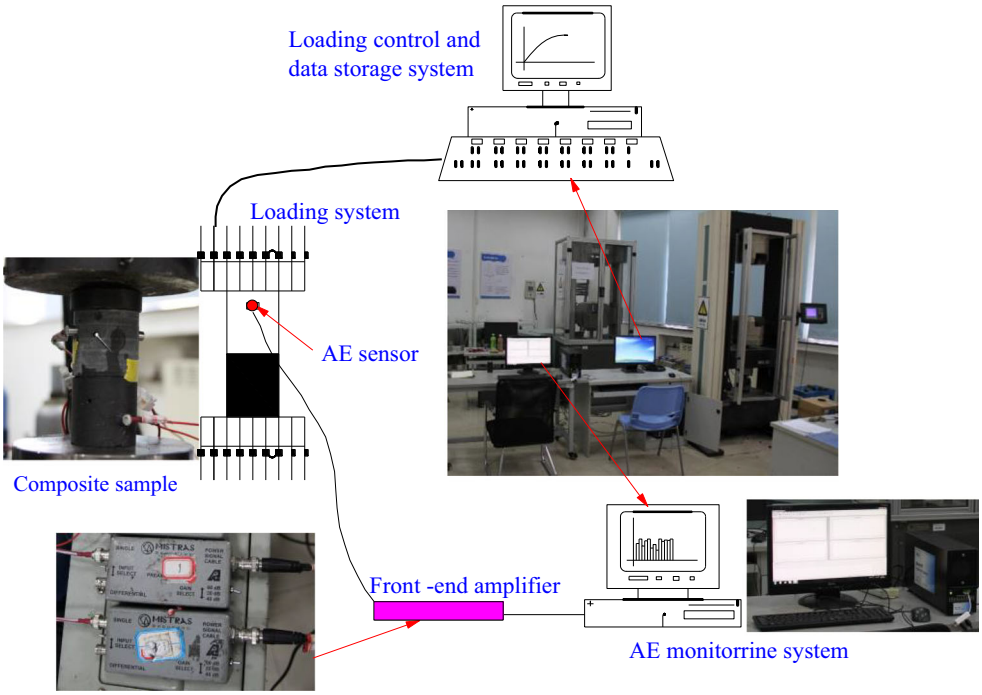

Fig. 2 Overview of experiment setup

Significant investigations have been conducted on the strength and failure modes of "combined coal-rock mass" structures. For example, Petukhov and Linkov (1979) analyzed the post-peak stability of a roof-coal system. Chen et al. (2017) studied the influence of the uniaxial compressive strength of rock-coal height ratio on the roof and coal-mass structure, macro-damage crack-initiating stress and elastic modulus. The precursory information of uniaxial compression instability failure of sandstone-coal and sandstone-coal-mudstone was compared by Zhao et al. (2008) using infrared thermography, acoustic emission (AE) and strain monitoring. Huang and Liu (2013) researched the influence of the loading rate on the mechanical properties of combined coal-rock. Liu et al. (2015) studied the effect of strength on the failure pattern and mechanical behaviour of a rock-coal-rock combined specimen. Guo et al. (2011) and Zhao et al. (2016) studied the strength and failure mechanism of combined coal-rock mass with different dip angles. Zhang et al. (2012) studied how three combinations (rock-coal-rock, rock-coal and coal-rock) affect the mechanical properties and failure characteristics of coal-rock composites. Zuo et al. (2016) studied the mechanical properties and failure characteristics of coal-rock composites under different stress states. Finally, Lu (2008) studied rock-coal height ratio affect coal-rock composites, including "roof and coal seam", "coal seam and basic roof", "coal seam and immediate roof" and "floor, coal seam, basic roof".

The research discussed above is of great significance to understand the strength and failure characteristics of combined coal-rock strata. However, these studies focus on intact combined coal-rock, whereas few studies deal with combined coal-rock with fractures. In a recent paper, Yin et al. (2018) studied the strength and failure characteristics of combined coal-rock with interior penetration and single fracture in a coal seam and analyzed how fracture angle affects the mechanical properties of coal-rock composite failure. Chen et al. (2019) used a numerical simulation to analyse how the loading rate affects uniaxial compression failure of combined coal-rock. However, no reports are yet available on how pre-conditioned cracks in the rock affect the mechanical properties of combined coal-rock. Thus, the present work studies how artificially induced rock cracks affect the mechanical properties and failure modes of combined coal-rock under uniaxial compression. The research is essential for guiding hydraulic fracturing to weaken hard roofs, and therefore reducing the risks of windblasts, rockbursts and outbursts.

Experiment setup

Specimen preparation

Lump rock samples were taken from the 3107 working face of Shenshuban Coal Mine in Yulin city, Shanxi. Roof mudstone and coal were selected and cored into standard cylindrical specimens, with a diameter of 50 mm and a height of 50 mm, respectively. The adhesives, such as super glue (502 glue) (Huang and Liu 2013), the AB adhesive (Liu et al. 2004) and modified acrylate adhesive (Gong et al. 2018), are often used in the manufacture of coal-rock-combined specimen. Therefore, the super glue (502 glue) was selected in the paper. Then, the rock and coal specimens were bonded with glue

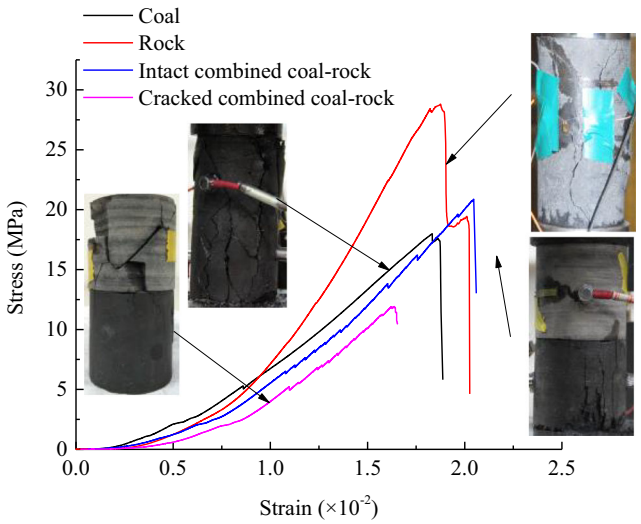

Fig. 3 Mechanical properties of coal, rock, intact combined coal-rock and cracked combined coal-rock

(Fig. 1a) to form a combined coal-rock specimen. The sizes and parallelism of the combined coal-rock specimens were determined and checked by a caliper, a right-angle ruler, a horizontal test platform, dial indicators and a dial-indicator rack, respectively. The combined specimen met the following requirement: (1) the two end-planes of the specimen need to be parallel and should not deviate by more than 0.05 mm, (2) the area of the two ends of the specimen should not be different by more than 0.2 mm and (3) the two ends of the specimen should be perpendicular to the axis of the specimen.

High-pressure water-jet cutting was used to cut the rock part of the combined coal-rock specimen to create cracks at a certain length and angle, as shown in Fig. 1(b). Each crack aperture was 0.5 mm wide. Figure 1(c) shows an overview of 21 combined coal-rock specimens with various pre-existing cracks to be tested in this research. The intact specimen of combined coal-rock with no fractures was used as a reference group. For this physical sample, the fracture angle is usually set to 0° to 90°. When the fracture angle is set at 45°, the failure mode of model is obvious and easily discernible. It is convenient to observe the influence of fracture trace length on the mechanical properties and failure mechanism of the model. Additionally, non-penetrated cracks exist more widely in nature; therefore, the crack length was set as 30 mm to make on-penetrated crack samples. Therefore, crack specimens can be categorized into two groups: (1) the crack angle was fixed at $\theta = 45°$, and the crack lengths L were set as 5 mm, 15 mm, 25 mm, 30 mm, 40 mm and 50 mm; (2) the crack length L was fixed at 30 mm, and the crack angles were set as 0°, 15°, 30°, 45°, 60°, 75° and 90°.

Experiment procedure

The DAW-300 rock mechanics testing system is used for combined specimen testing, which is shown in Fig. 2. The 24-channel Acoustic Emission (AE) system (American Acoustic Company, USA) is used to monitor the entire loading process. Two NANO-30 sensors with a working frequency ranging from 35 to 100 kHz and a resonance frequency of 55 kHz are used to record AE signals. The peak frequency of the sensor is 268.55 kHz, and the threshold value, the gain, the lower limit of the analogy filter, the upper limit and the sampling frequency are set as 45 dB, 40 dB, 1 kHz, 400 kHz and 20 kHz. The combined coal-rock specimens are placed on the loading frame under uniaxial loading rate at 0.5 mm/min until failure occurs.

Analysis of experiment results

Analysis of mechanical properties of coal-rock

A serious of uniaxial compression tests is conducted on intact mudstone, pure coal, intact combined coal-rock and cracked combined coal-rock specimens to obtain the stress-strain curves and mechanical parameters of the four materials, as seen in Fig. 3. Results show that the strength and elastic modulus of rock > intact combined coal-rock > coal > cracked combined coal-rock. Overall, the mechanical properties of the intact combined coal-rock are in between that of pure coal-rock, but the existence of crack has weakened the strength and deformation behaviour of intact combined coal. Additionally, the triaxial compression tests are carried out for the intact mudstone and pure coal, and the corresponding mechanical parameters are given in Table 1.

Failure process and acoustic emission of combined coal-rock specimens with pre-existing cracks

An intact specimen and five pre-conditioned crack specimens were selected to demonstrate their stress-strain curves and AE characteristics, as shown in Fig. 4. The graph shows that the stress-strain curves for the intact specimen and crack

Table 1 Mechanical parameters of the intact rock and coal

Material type	Peak strength (MPa)	Elastic modulus (GPa)	Friction angle (°)	Cohesion (MPa)
Rock	28.807	2.832	31	3.2
Coal	17.986	1.465	19	0.8

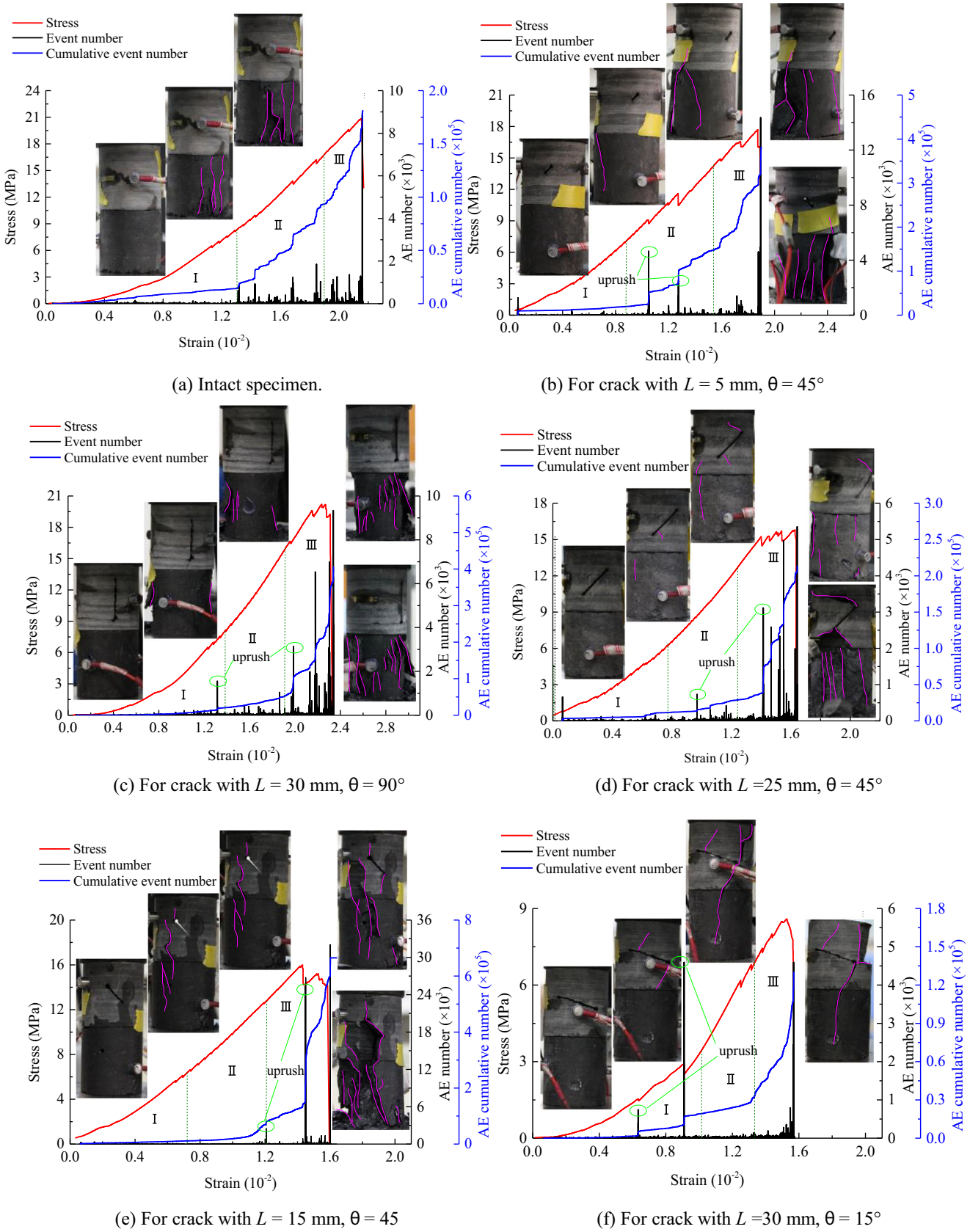

(a) Intact specimen.

(b) For crack with L = 5 mm, θ = 45°

(c) For crack with L = 30 mm, θ = 90°

(d) For crack with L =25 mm, θ = 45°

(e) For crack with L = 15 mm, θ = 45

(f) For crack with L =30 mm, θ = 15°

Fig. 4 Failure process and AE of combined coal-rock specimens with cracks. **a** Intact specimen. **b** For crack with $L = 5$ mm, $\theta = 45°$. **c** For crack with $L = 30$ mm, $\theta = 90°$. **d** For crack with $L = 25$ mm, $\theta = 45°$. **e** For crack with $L = 15$ mm, $\theta = 45°$. **f** For crack with $L = 30$ mm, $\theta = 15°$

specimens are similar to each other, which can be divided into four stages: compaction stage, linear elastic stage, plastic stage and damage stage. The first three stages are determined (Cai 2010; Gong and Wu 2020) and labelled as I, II and III in Fig. 4.

With increasing axial strain, a clear correspondence between AE and various stages of stress-strain curves for combined coal-rock specimens can be observed. At the compaction stage, there is few AE events and weak energy release, which indicates that few fractures occurred in the specimen. Then, at the linear elastic stage, the number of AE events as well as AE energy begins to increase slightly, which indicates the initiation of micro-cracks within the specimens. Moreover, at the plastic stage, both the number of AE events and the energy release increases significantly, indicating a significant increase in the number of cracks, which corresponds to the rapid growth and extension of micro-cracks. Finally, when the peak strength is reached, the number of AE events increases rapidly, accompanied by a sudden release of a large amount of energy, which indicates that a large number of micro-cracks are rapidly generated, propagated and coalesced into macro-cracks and leads to the failure of whole specimens.

Figure 4 shows the failure process of the specimen during various stages of loading. A comparison among the intact specimen (Fig. 4(a)), specimen with a 5-mm long and 45° angle crack (Fig. 4(b)) and specimen with a 30-mm long and 90° angle crack (Fig. 4(c)) shows that the failure process is similar for the three cases. Upon loading these specimens, cracks first initiates in the coal, and then propagates and coalesces until the coal is completely fractured by tensile stress. However, cracks in the coal could not penetrate to the rock, and thus, the rock remains intact. For the specimen with a 25-mm long and 45° angle crack and the specimen with a 15-mm long and 90° angle crack, as plotted in Fig. 4d and e, they share a similar failure process. The cracks initiate roughly at the same time in the combined coal-rock. Both wing and branching cracks appear at the tip and periphery of the pre-set crack in the rock, whereas tensile cracks appear in the coal. Upon increasing axial loading, cracks expand independently in the combined coal-rock, and some rock cracks penetrate into the coal. For the specimen with the 30-mm long and 15° angle crack, as seen in Fig. 4(f), the cracks initiate preferentially along pre-set cracks, then secondary cracks and wing cracks occur at the tip of the pre-set cracks, which eventually lead to rock shear failure.

Figure 4 shows that the number of micro-cracks released in the elastic-plastic stage increases steadily for the intact specimen. On the other hand, for the pre-conditioned specimens, the number of micro-cracks increased is in a bumpy and discontinuous manner when the specimen enters the plastic deformation stage. This is because the pre-set cracks have changed the gradual process from micro-crack propagation to throughout penetration in the plastic stage, which is predominated by the sudden coalesce between micro-cracks and pre-set cracks.

Effect of crack length and angle on the stress-strain curves of combined coal-rock specimens

Figure 5 shows the stress-strain curves of pre-conditioned specimens with various crack lengths and angles. Results show that the peak strength decreases gradually with increasing crack length, and the slope of the stress-strain curve gradually becomes gentle, as plotted in Fig. 5(a). The stress-strain curve in Fig. 5(b) first flattens and then steepens as the crack angle θ increases from 0° to 90°. The shortest stress-strain curve of the specimen is for the $L = 50$ mm and 30° pre-set crack. Moreover, the strain intervals corresponding to the compaction stages of the specimens do not vary significantly in different

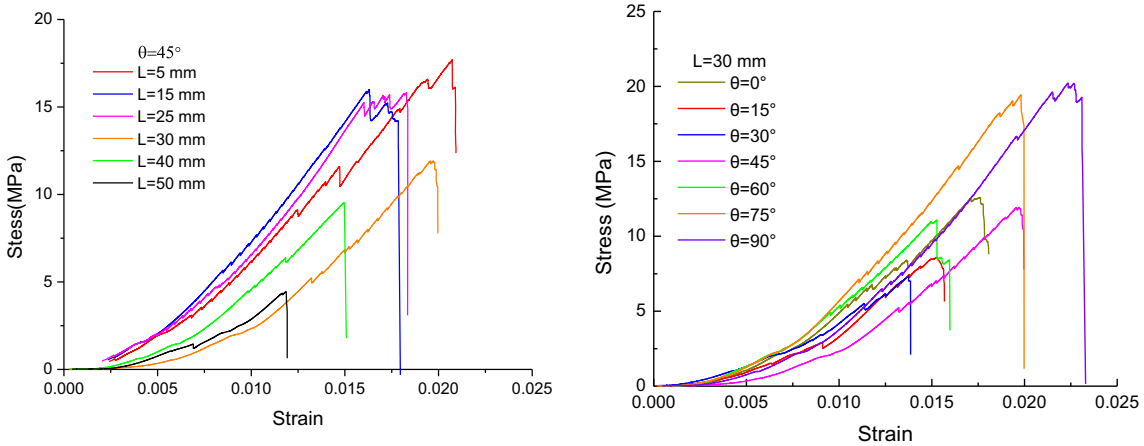

(a) Cracklength (b) Crackangle

Fig. 5 Stress-strain curves of combined coal-rock specimens as a function of (**a**) crack length and (**b**) crack angle

Table 2 Mechanical parameters of combined specimen

Crack angle (°)	Crack length L (mm)	Elastic modulus (GPa)	Peak strength (MPa)	Peak strain	Crack length L (mm)	Crack angle (°)	Elastic modulus (GPa)	Peak strength (MPa)	Peak strain
Intact	–	1.4086	20.866	0.022	30	0	1.020	12.585	0.018
45	5	1.115	17.687	0.019	30	15	0.811	8.596	0.015
45	15	1.257	15.997	0.014	30	30	0.735	7.3464	0.011
45	25	1.080	13.667	0.012	30	45	1.000	11.922	0.016
45	30	1.000	11.922	0.016	30	60	1.067	11.085	0.015
45	40	0.762	9.537	0.015	30	75	1.399	19.430	0.020
45	50	0.520	4.449	0.012	30	90	1.359	20.225	0.022

specimens, whereas the strain intervals corresponding to the elastic-plastic stage are clearly different. Moreover, as the pre-set crack length increases or the crack angle approaches 30°, the strain interval of the specimen in the elastic-plastic stage decreases, which indicates that these specific configurations of pre-set cracks can accelerate the transition of entire specimens from micro-scale cracking to macro-scale failure.

Effect of crack length and angle on the mechanical parameters of combined coal-rock specimens

Table 2 shows the average mechanical parameters of the specimen of intact combined coal-rocks and combined coal-rocks with the fracture. Figure 6 gives the results of uniaxial compression measurements of combined coal-rocks with pre-set cracks of different lengths. The results show that the elastic

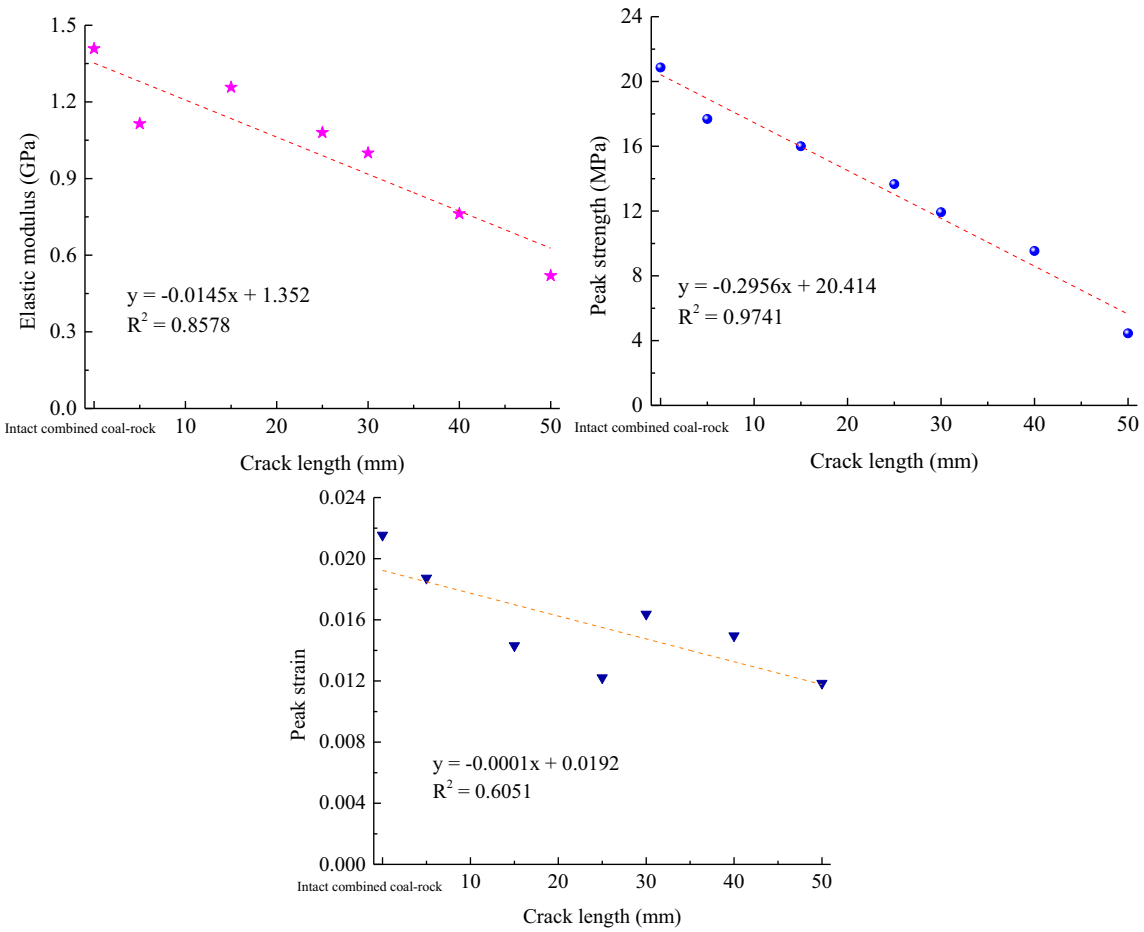

Fig. 6 Strength and deformation as a function of crack length in the combined coal-rock specimens

modulus, peak strength and peak strain of the combined coal-rock specimens decrease linearly with increasing crack length. The relationship between the elastic modulus and crack length can be described by a linear relationship $y = -1444.97x + 1352$, where the elastic modulus decreases from 1.338 GPa (intact combined coal-rock) in the intact specimen to 0.519 GPa in the specimen with a 50-mm crack by 61.2%. The relationship between the peak strength and crack length can be fitted by $y = -2.9561x + 20.414$, where the peak strength decreases from 20.865 MPa in intact combined coal-rock to 4.449 MPa in the specimen with a 50-mm crack (a decrease of 78.7%). Finally, the fit between the peak strain and crack length follows $y = -0.0015x + 0.0192$, where the peak strain decreases from 0.0215 in the intact specimen to 0.0118 in the specimen with a 50-mm crack by 45.1%.

Figure 7 shows the results of uniaxial compression measurements of combined coal-rocks specimens with cracks of different angles. With the increasing crack angle, the elastic modulus, peak strength and peak strain of the combined coal-rock specimen show approximately U-shaped, and have apparent anisotropy. Compared with the intact specimen, the maximum and minimum values of elastic modulus of the combined coal-rock specimen of decrease are 45.1% and 0.7% in 30° and 75° crack angle (as plotted in Fig. 7(a)), respectively. To the peak strength, the maximum and minimum values of decrease are 64.8% and 3.1% in 30° and 75° crack angle (as plotted in Fig. 7(b)), respectively. Besides, the maximum and minimum values of decrease are 48.2% and −9.2 (increase) in 30° and 90° crack angle for peak strain (as plotted in Fig. 7(c)), respectively. Results show that the elastic modulus, peak strength and peak strain of combined coal-rock specimen are almost equal to those of the intact specimen when the cracks are oriented at $\theta = 75°$ and 90°. The elastic modulus, peak strength and peak strain of combined specimens reach their minimum values as θ approaches to 30°.

The longer the artificial crack is, or the closer the crack angle is to 30°, the reduction in elastic modulus, peak strength and peak strain become larger for the combined coal-rock specimens, and the better weakening effect induced by the pre-conditioned cracks. This observation can be explained by that longer cracks have a larger discontinuous surface, which is easier to trigger sliding failure. In addition, according to the Mohr-Columbus failure criterion, given that the angle of

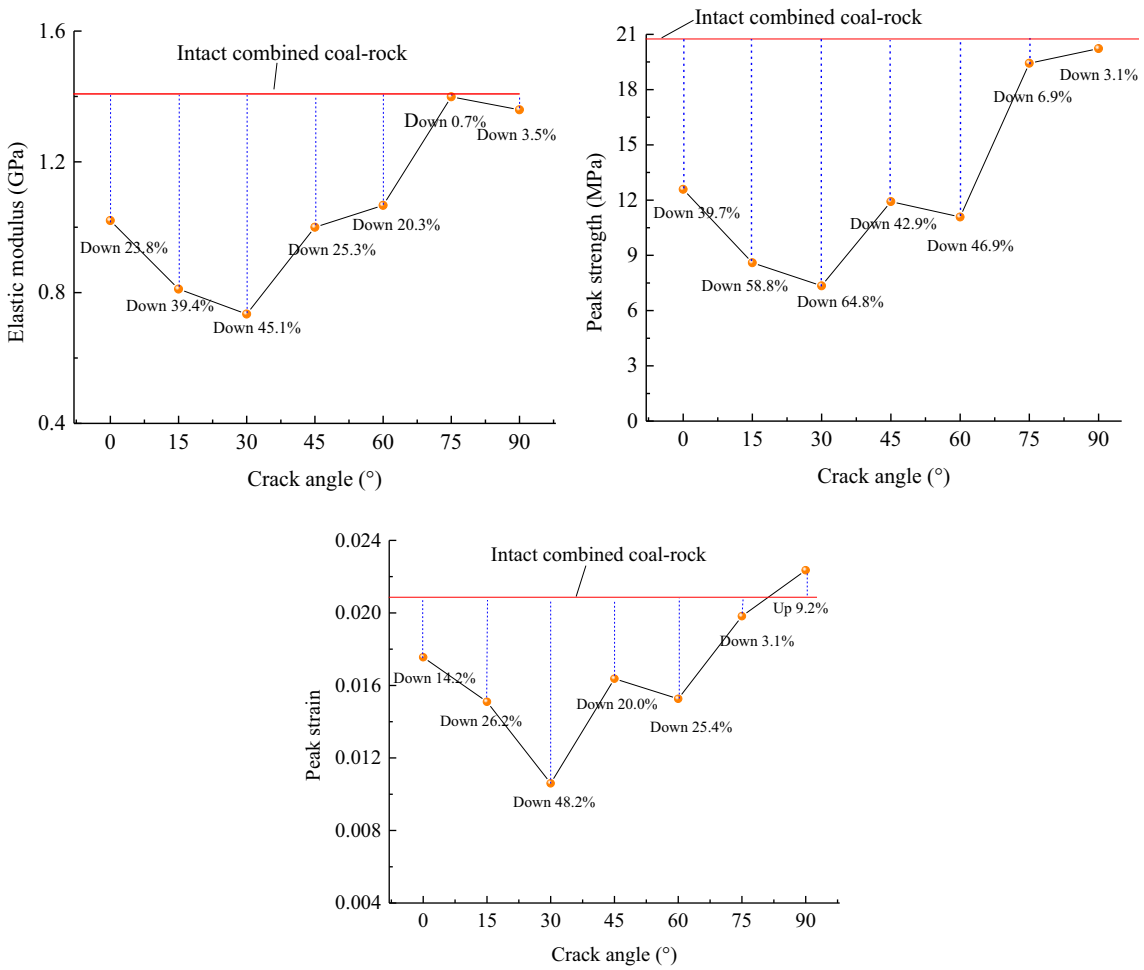

Fig. 7 Strength and deformation of a combined coal-rock specimen as a function of crack angle

internal friction for roof rock is approximately 31° (as shown in Table 1), the weakest plane for the pre-conditioned crack to initiate shear failure is at the 45° minus half of internal friction angle, which suggests that the 30° crack angle is the weakest plane.

Effect of crack length and angle on the AE of combined coal-rock specimens

The measurement results of AE for combined coal-rock specimens with different crack lengths is shown in Fig. 8. Results show that, with the increase of axial strain, there is no micro-crack initially and then followed by rapid growth of micro-cracks as indicated by the number and energy release of AE. The number of cumulative events and cumulative energy of AE for the intact specimen is higher than pre-conditioned specimens. Furthermore, as the crack length L increases from 5 to 50 mm, the number of AE cumulative events decreases from 0.65 to 83.2%, and the cumulative energy decreases from 20.5 to 84.7% (as shown in Table 3). This indicates that, with increasing crack length, the number of cumulative events and the cumulative energy of AE both decreases gradually. The number of AE events and energy release at the moment of specimen failure for various crack lengths is summarised in Fig. 8(c), which also presents a similar trend.

Figure 9 shows the cumulative event number and cumulative energy release of AE for the intact specimen and specimens with various crack angles during the entire loading process. As the crack angle θ increases from 0° to 90° in 15° steps, the cumulative number of AE events decreases respectively by 35.6%, 66.1%, 68.8%, 58.3%, 48.1% and 28.5% and increases by 5.6%. Furthermore, as the crack angle θ increases from 0° to 90° in every 15° steps, the cumulative AE energy decreases respectively by 37.7%, 71.7%, 81.7%, 65.9%,

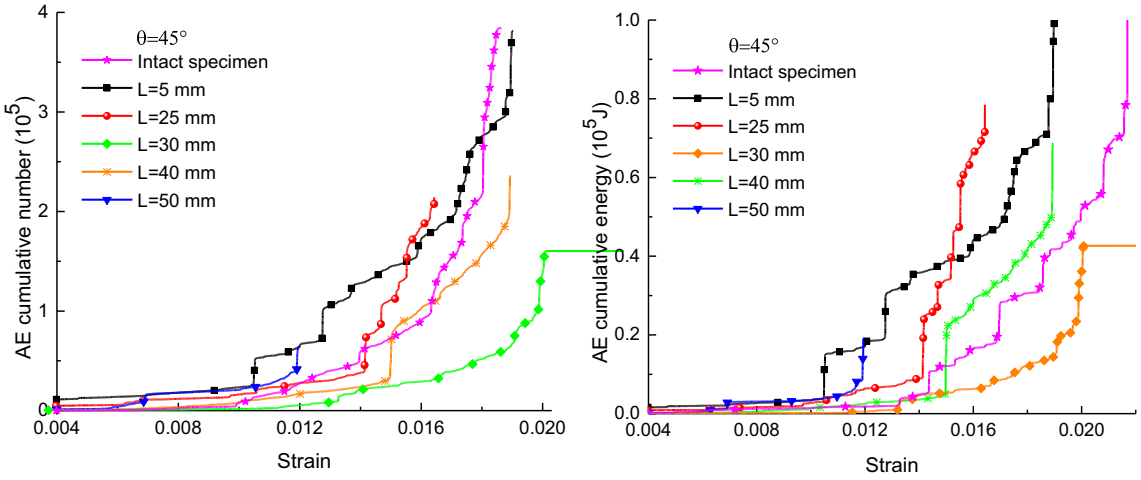

(a) Cumulative event number of AE

(b) Cumulative event energy of AE

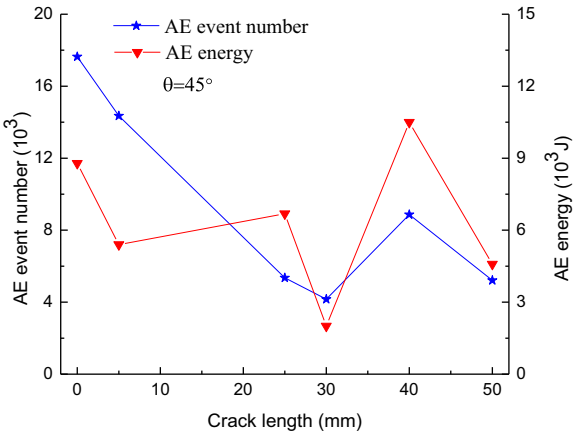

(c) AE at the moment of specimen failure as a function of crack length

Fig. 8 Effect of crack length on AE during the entire loading process. **a** Cumulative event number of AE. **b** Cumulative event energy of AE. **c** AE at the moment of specimen failure as a function of crack length

Table 3 Statistics of cumulative number and cumulative energy of AE for combined specimens with different crack lengths

Crack length L (mm)	Crack angle θ (°)	Cumulative event number (10^5 J)	Decrease (%)	Cumulative energy release (10^5 J)	Decrease (%)
Intact	-	3.841	-	1.251	-
5	45	3.816	− 0.65	0.995	− 20.5
25	45	2.142	− 44.2	0.785	− 37.3
30	45	1.603	− 58.3	0.427	− 65.9
40	45	2.362	− 38.5	0.688	− 45.0
50	45	0.647	− 83.2	0.192	− 84.7

35.6% and 17.1% and increases by 15.3% (seen in Table 4). These results show that, as the crack angle θ increases from 0° to 90°, the cumulative number of AE events and the cumulative energy first decrease and then increase. The minimal cumulative number of events and cumulative energy occur for the specimens with 30° and 45°cracks. A more straightforward variation trend can be found in Fig. 9(c), where the number of AE events and the AE energy at the moment of specimen failure was plotted against the change of crack angles.

The above experiment results suggest that the longer the artificial crack is, or the closer the crack angle is to 30°, the fewer micro-cracks and the less energy released during the whole loading process, and the few number of micro-cracks

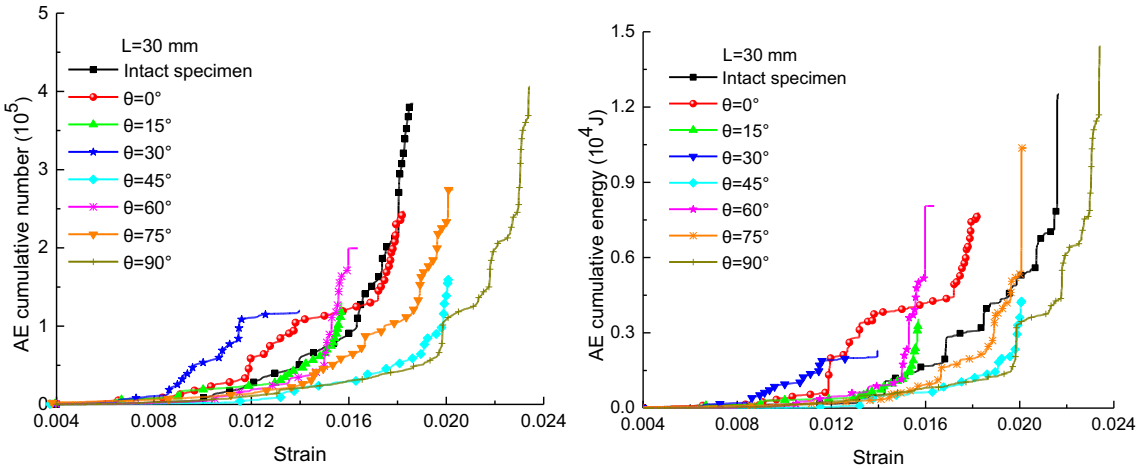

(a) Cumulative number of acoustic events

(b) Cumulative acoustic-event energy

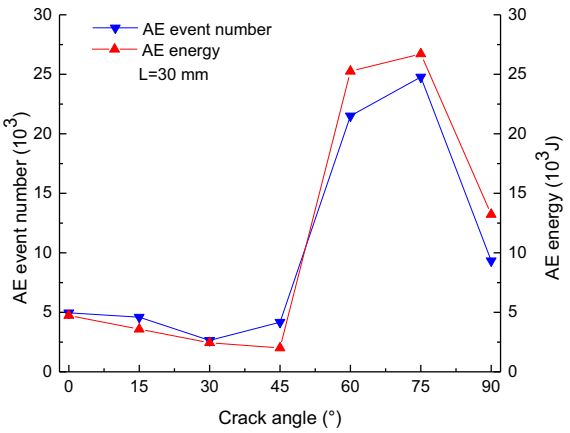

(c) AE at the moment of specimen failure as a function of crack angle

Fig. 9 Effect of crack angle on AE over the entire loading process. **a** Cumulative number of acoustic events. **b** Cumulative acoustic-event energy. **c** AE at the moment of specimen failure as a function of crack angle

Table 4 Statistics of the cumulative number of AE events and cumulative AE energy for combined specimens with various crack angles

Crack angle θ (°)	Crack length L (mm)	Cumulative number (10^5)	Decrease (%)	Cumulative energy (10^5 J)	Decrease (%)
Intact	-	3.841	-	1.251	-
0°	30	2.473	− 35.6	0.779	− 37.7
15°	30	1.301	− 66.1	0.354	− 71.7
30°	30	1.199	− 68.8	0.229	− 81.7
45°	30	1.600	− 58.3	0.427	− 65.9
60°	30	1.995	− 48.1	0.806	− 35.6
75°	30	2.746	− 28.5	1.037	− 17.1
90°	30	4.058	+ 5.6	1.443	+ 15.3

and the energy released at the moment of failure. This indicates that the micro-macro-damage caused by the artificial crack has the trend of changing from acuteness to moderation during the loading process.

Effect of crack length and angle on crack-initiating modes and stress of combined coal-rock specimens

Crack-initiating stress

When the stress at the tip of a crack reaches the critical stress, micro-cracks begin to appear, corresponding to the starting point of the linear elastic stage in Fig. 4. The stress at this point is called the crack-initiating stress σ_c and corresponds to the point at which the original crack inside the rock is compacted, and the new crack initiates and begins to propagate.

Figure 10(a) shows the crack-initiating stress of specimens as a function of crack length. The crack-initiating stress of the intact specimen is the highest (6.371 MPa). Compared with the stress in the intact specimen, the crack-initiating stress in the specimen with various fracture trace decreases by 0.69%, 0.59%, 8.37%, 18.34%, 52.40% and 77.13%, respectively. This indicates that the crack-initiating stress decreases gradually with increasing crack length.

Figure 10(b) shows the crack-initiating stress of specimens as a function of crack angle. When θ ranges from 0° to 90° in 15° steps, the crack-initiating stress of the specimen decreases by 17.1%, 39.6%, 52.1%, 45.0%, 16.3%, 1.6% and 0.1%, respectively, compared with that of the intact specimen. This shows that, as θ increases, the crack-initiating stress of the specimen first decreases and then increases, with the minimum crack-initiating stress occurring at $\theta = 30°$.

Crack-initiating modes

Figure 11(a) shows the crack-initiating process of specimens with various crack lengths. The crack-initiating process of the

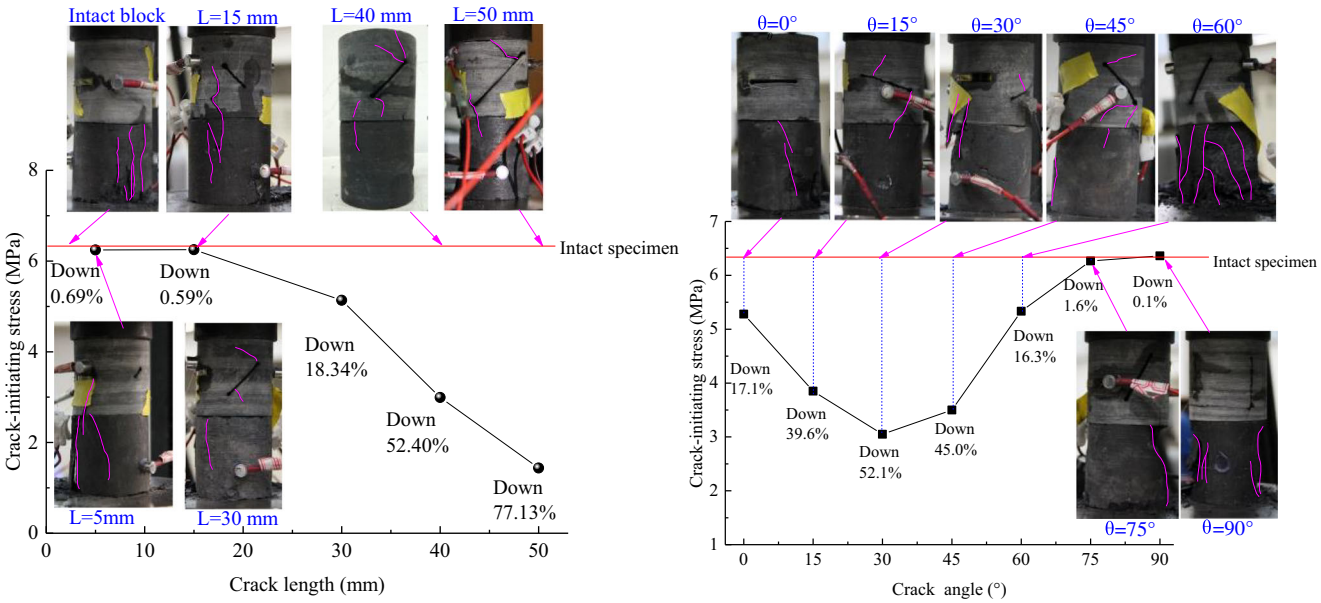

Fig. 10 Crack-initiating modes and stress as a function of (**a**) crack length and (**b**) crack angle

specimen with $L = 5$ mm is similar to that of the intact specimen. Upon loading the specimen, the crack is first initiated in the coal. The crack initiation processes for specimens with $L = 15$ mm and $L = 30$ mm are both similar. The cracks initiate basically at the same time in the combined coal-rock. Both wing and branching cracks appear at the tip and periphery of the pre-set crack in the rock, whereas tensile cracks appear in the coal. The crack-initiating process of the specimen with $L = 40$ mm is similar to that of the specimen with $L = 50$ mm. In both specimens, the cracks initiate preferentially along pre-set cracks, secondary cracks and wing cracks that occur at the tip of the pre-set cracks, causing rock shear failure.

The crack-initiating process of specimens is shown in Fig. 11(b) for different crack angles. Upon loading a specimen

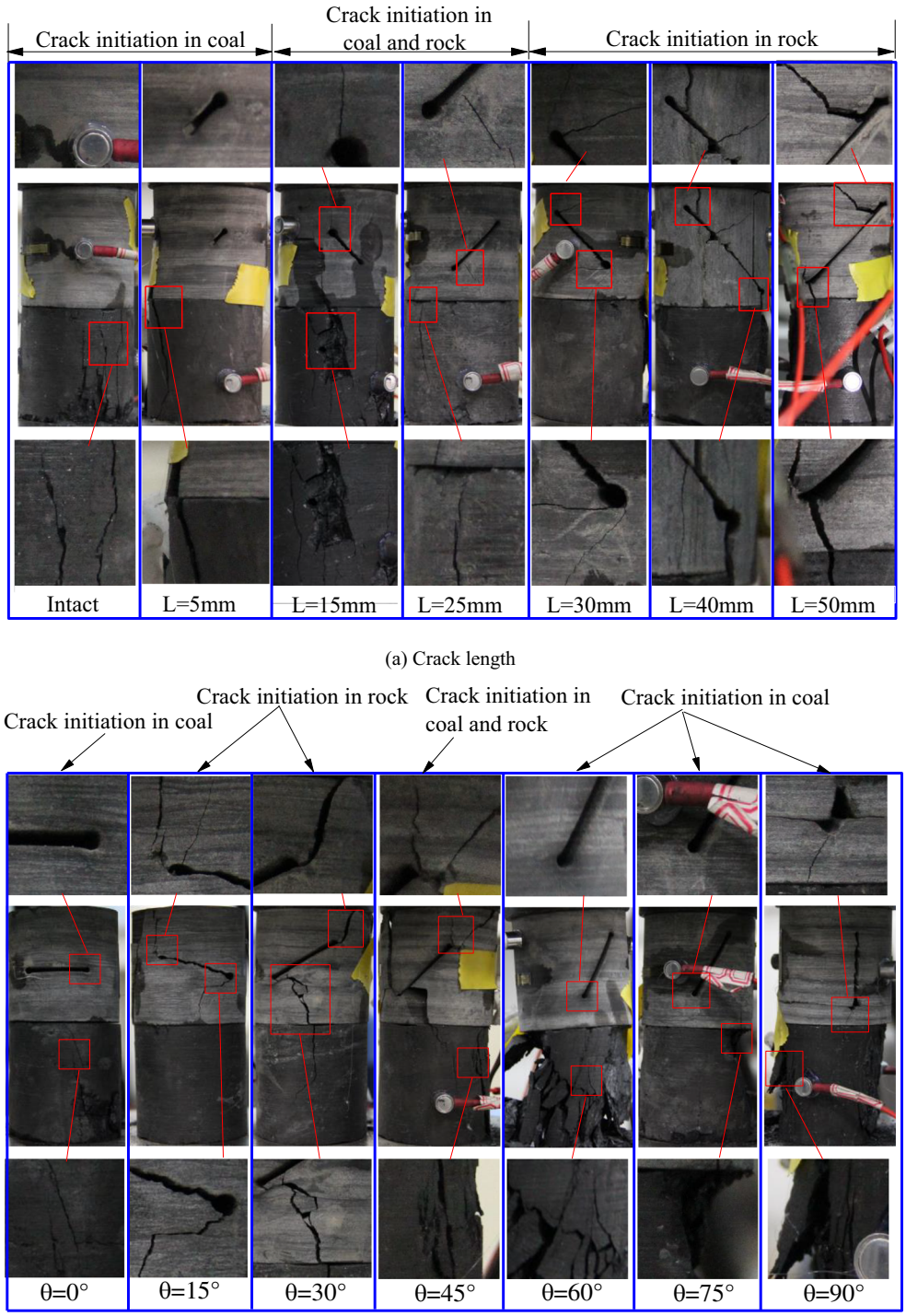

Fig. 11 Effect of crack length and angle on crack initiation characteristics and failure modes of combined coal-rock specimens. **a** Crack length. **b** Crack angle

with $\theta = 0°$, the crack first initiated in the coal. The crack-initiating processes of specimens with $\theta = 15°$and $\theta = 30°$ are similar: both are preferentially initiated in the middle and the tip of pre-set cracks, secondary cracks and wing cracks, thereby causing shear failure of the rock. Upon loading the specimen with a pre-set crack at $\theta = 45°$, cracks are simultaneously initiated in both combined coal-rock. Both wing and branching cracks appear at the tip and periphery of the pre-set crack in the rock, and tensile cracks appear in the coal. The crack-initiating processes of specimens with $\theta = 60°$, $\theta = 75°$ and $\theta = 90°$ are all similar, where cracks first initiate in the coal.

These experimental results show that an increase in crack length or a gradual approach of the crack angle to 30° leads to one of three crack-initiating modes in the specimens:

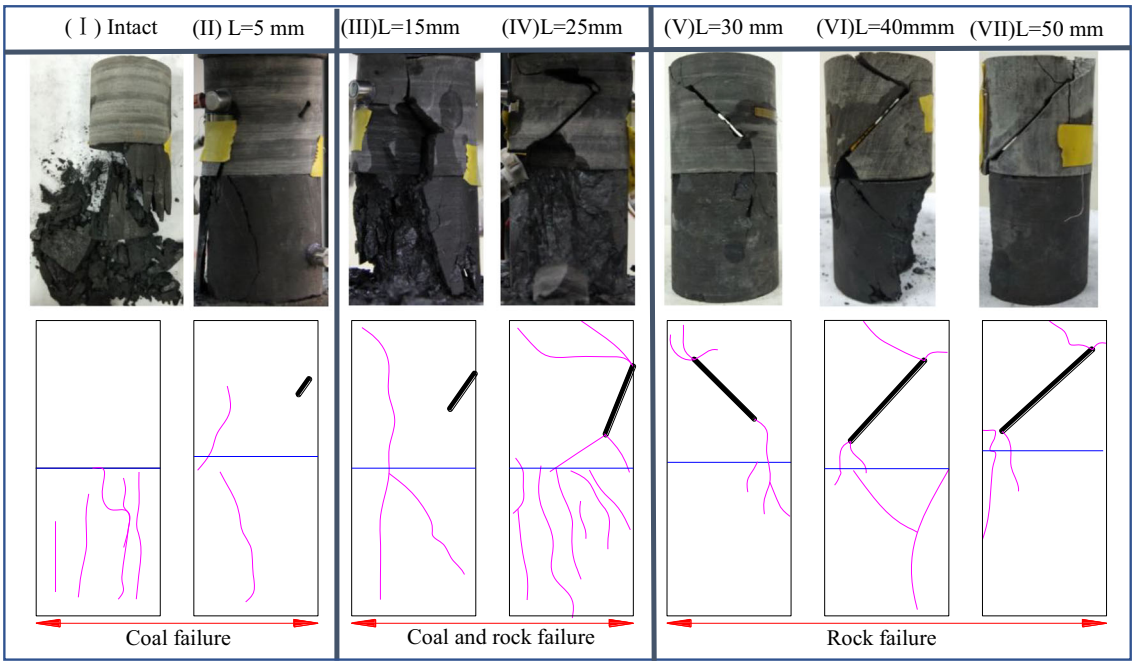

(a) Crack length

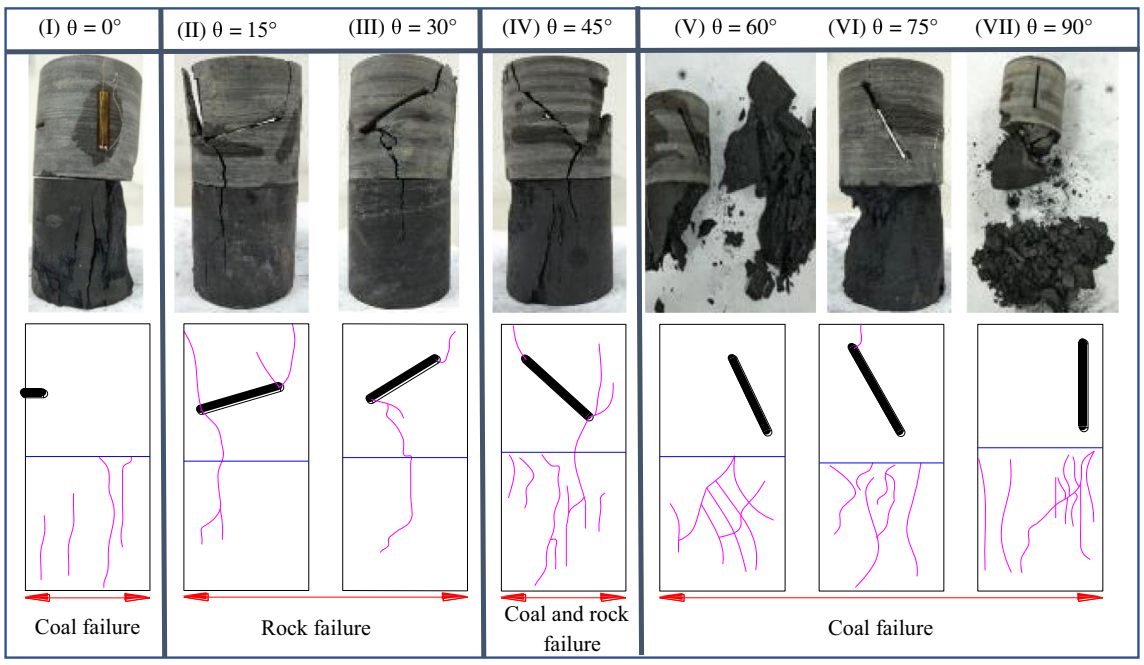

(b) Crack angle

Fig. 12 Effect of crack length and angle on failure characteristics and failure modes of combined coal-rock. **a** Crack length. **b** Crack angle

preferential crack initiation in coal, simultaneous crack initiation in combined coal-rock and preferential crack initiation in rock.

Effect of crack length and angle on failure characteristics and failure modes of combined coal-rock specimens

Figure 12(a) shows how the crack length affects the failure characteristics of specimens. With increasing pre-set crack length, the failure mode varies from coal failure only to coal-and-rock failure and finally to rock failure only. After loading the intact specimen and a specimen with a crack length $L = 5$ mm, the rock did not break, but the coal was severely damaged. Moreover, the fragments were found to be small and uniform with a high degree of breakage, which indicates that the failure mode of the specimen is mainly coal failure, as seen in Figs. 12a (I) and 12a (II)). The damage was observed in both combined coal-rock parts for the specimens with crack lengths of $L = 15$ mm and 25 mm: the rock part presented shear failure along the pre-conditioned cracks while coal presented predominately tension failure. Furthermore, the fragments increased in size but decreased in number, as plotted in Figs. 12a (III) and 12a (IV). For specimens with pre-set crack lengths $L = 30$, 40 and 50 mm, rock shear failure along the cracks was observed and some of these shear cracks even penetrated to the coal part. However, no tensile failure appeared in coal, and the shape of the coal part remained relatively intact. These results indicate that rock failure is the main failure mode for the combined coal-rock specimens, as shown in Figs. 12a (V), 12a (VI) and 12a (VII).

Figure 12b shows how the crack angle affects the failure mode of various specimens. As the pre-set crack angle varies from 0° to 90° in every 15° steps, the specimen failure mode ranges from coal failure to rock failure to coal-and-rock failure and finally to coal failure. After loading the specimen with a pre-set crack angle at $\theta = 0$, the rock did not break, but the coal was severely damaged with a high degree of breakage. Furthermore, the coal fragments are small and uniform, which indicates that the failure mode of specimen is mainly tensile failure of the coal part, as seen Fig. 12b (I). After loading the specimen with pre-set cracks at $\theta = 15°$ and 30°, rock presented a shear failure along the pre-set cracks, which also penetrated into the coal part. On the other hand, no tensile cracks were observed in the coal and the shape of coal remained relatively intact. This indicates that rock failure is the main failure mode for the combined coal-rock specimen, as shown in Figs. 12b (II) and 12b (III). Damage was observed in both combined coal-rock parts for the specimens with pre-set crack angles at $\theta = 45°$: shear failure was observed in the rock along the pre-set cracks and tensile presented in the coal part. In addition, the fragments are larger and fewer compared with other angles, as plotted in Fig. 12b (IV). Upon loading the specimen with pre-set cracks at $\theta = 60°$–90°, the rock did not break, but the degree of coal breakage was severe, and the fragments were small and uniform, which indicates that the failure mode of the specimen is primary tensile failure in the coal, as seen in Figs. 12b (V), 12b (VI) and 12b (VII).

The experiment results show that, upon gradually enlarging the length of pre-set cracks or having the crack angle approach 30°, the specimen can experience one of three typical failure modes: coal failure, coal-and-rock failure and rock failure. The final fracture mode of combined coal-rock with pre-conditioned cracks is closely related to the crack parameters: the crack angle mainly affects the location of the crack initiation, and the crack length mainly affects the fracturing degree of the specimen. Therefore, in terms of pre-fracturing roof rock to control excessive roof strata stress and promote continuous roof fracturing and collapse, the artificial crack length and orientation must be optimised. Note that rock shear cracks often penetrate into and damage the coal, but the coal cracks cannot penetrate into the rock.

Conclusion

This research focuses on understanding the impact of crack length and crack angle on weakening roof-coal strata through multiple uniaxial tests in the laboratory. Some of the key findings are summarised below:

(1) By increasing the length of pre-conditioned cracks, or as the crack angle gradually approaches 30°, the stress-strain curve of combined coal-rock specimens tends to be gentler. The range of the elastic modulus decreases, the peak strength and peak strain increase and the strain interval corresponding to the elastic-plastic stage decreases. These results indicate that the artificial crack weakens the mechanical properties of the combined coal-rock and accelerates the transition from micro-crack to macro-damage of the specimen.

(2) In combined coal-rock, the number of acoustic-emission events and their energy clearly correspond with the stress-strain curve. When the specimen enters the plastic deformation stage, the number of acoustic emissions increases with the jump style. For long pre-set cracks or crack angles close to 30°, the cumulative number of micro-cracks and the cumulative energy released over the entire loading process decrease gradually, and the number of micro-cracks and the energy released at the moment of failure also decrease. These results indicate that the transition from micro-crack to macro-damage in the specimen starts to quiet down.

(3) With increasing pre-conditioned crack length or as the crack angle approaches 30°, the crack-initiating stress in the combined coal-rock specimen gradually decreases via one of three crack-initiating modes: preferential crack

initiation in coal, simultaneous crack initiation in combined coal-rock and preferential crack initiation in rock. Thus, three typical failure modes are possible: coal failure, combined coal-rock failure and rock failure.

(4) To reduce the risk of hazards caused by hard roofs and improve the effectiveness of pre-conditioned fractures to weaken these roofs, the length and orientation of artificial cracks should be well controlled and optimized.

Funding This work was supported by the Fundamental Research Funds for the Central Universities (2018XKQYMS10), Regional Joint Fund for Basic and Applied Basic Research Fund of Guangdong Province (2019A1515110836) and China Postdoctoral Science Foundation Project (2019M662918).

Data availability The data used to support the findings of this study are available from the corresponding author upon request.

Compliance with ethical standards

Conflict of interest The authors declare that they have no conflicts of interest.

References

Cai M (2010) Practical estimates of tensile strength and Hoek-Brown strength parameter mi of brittle rocks. Rock Mech Rock Eng 43: 167–184

Cai W, Dou LM, Si GY, Cao AY (2016) A principal component analysis/fuzzy comprehensive evaluation model for coal burst liability assessment. Int J Rock Mech Min Sci 100(81):62–69

Chen SJ, Yin DW, Jiang N, Wang F, Guo WJ (2019) Simulation study on effects of loading rate on uniaxial compression failure of composite rock-coal layer. Geomech Eng 17(4):333–342

Chen SJ, Yin DW, Zhang BL, Ma HF, Liu XQ (2017) Study on mechanical characteristics and progressive fail-ure mechanism of roof-coal pillar structure body. Chin J Rock Mech Eng 36(7):1588–1598

Guo DM, Zuo JP, Zhang Y, Yang RS (2011) Research on strength and failure mechanism of deep coal-rock combination bodies of different inclined angles. Rock Soil Mech 32(5):1333–1339

Gong FQ, Ye H, Luo Y (2018) The effect of high loading rate on the behaviour and mechanical properties of coal-rock combined body[J]. Shock Vib 6:1–9

Gong FQ, Wu C (2020) Identifying crack compaction and crack damage stress thresholds of rock using load–unload response ratio (LURR) theory[J]. Rock Mech Rock Eng 53(2):943–954

Huang BX, Liu JW (2013) The effect of loading rate on the behavior of samples composed of coal-rock. Int J Rock Mech Min Sci 61:23–30

Huang BX, Wang Y, Cao S (2015) Cavability control by hydraulic fracturing for top coal caving in hard thick coal seams. Int J Rock Mech Min Sci 74:45–57

Huang BX, Liu JW, Zhang Q (2018) The reasonable breaking location of overhanging hard roof for directional hydraulic fracturing to control strong strata behaviors of gob-side entry. Int J Rock Mech Min Sci 103:1–11

Kaiser PK (2012) Design of rock support system under rockburst condition. J Rock Mech Geotech Eng 4(3):215–227

Lin BQ, Li ZW, Zhai C, Bi Q, Wen YY (2011) Pressure relief and permeability-increasing technology based on high pressure pulsating hydraulic fracturing and its application. J Min Safety Eng 28(3):452

Lin BQ, Yan FZ, Zhu CJ, Zhou Y, Zou QL, Guo C, Liu T (2015) Cross-borehole hydraulic slotting technique for preventing and controlling coal and gas outbursts during coal roadway excavation. J Nat Gas Sci Eng 26:518–525

Liu B, Yang RH, Guo DM, Zhang DZ (2004) Burst-prone experiments of coal-rock combination at-1100 m level in Suncun coal mine[J]. Chin J Rock Mech Eng 23(14):2402–2408

Liu J, Wang EY, Song DZ, Wang SH, Niu Y (2015) Effect of rock strength on failure mode and mechanical behavior of composite samples. Arab J Geosci 8(7):4527–4539

Lu CP (2008) Strength weakening and alleviation principles of combined coal-rock and its application [D]. CUMT, Xuzhou, pp 79–84

Lu CP, Liu GJ, Liu Y, Xue JH, Zhang L (2015) Microseismic multi-parameter characteristics of rockburst hazard induced by hard roof fall and high stress concentration. Int J Rock Mech Min Sci 76:18–32

Mazaira A, Konicek P (2015) Intense rockburst impacts in deep underground construction and their prevention. Canadian Geotechnical Journal 52(10):1426–1439.

Ouyang ZH, Qi QX, Zhang Y, Wei XZ, Zhao SK (2011) Mechanism and experiment of hydraulic fracturing in rock burst prevention. Journal of the China Coal Society 36(S2):321–325

Petukhov IM, Linkov AM (1979) The theory of post-failure deformations and the problem of stability in rock mechanics. Int J Rock Mech Min Sci 16(2):57–76

Qiu SL, Feng XT, Zhang CQ, Xiang TB (2014) Estimation of rockburst wall-rock velocity invoked by slab flexure sources in deep tunnels. Can Geotech J 51(5):520–539

Qiu LM, Song DZ, He XQ, Wang EY, Li ZL, Yin S, Wei MH, Liu Y (2020) Multifractal of electromagnetic waveform and spectrum about coal rock samples subjected to uniaxial compression. Fractals 28(3):2050061

Si GY, Jamnikar S, Lazar J, Shi JQ (2015) Monitoring and modelling of gas dynamics in multi-level longwall top coal caving of ultra-thick coal seams. Part I: borehole measurements and a conceptual model for gas emission zones. Int J Coal Geomechan 144:98–110

Tan YL, Yu FH, Ning JG, Zhao TB (2015) Design and construction of entry retaining wall along a gob side under hard roof stratum. Int J Rock Mech Min Sci 100(77):115–121

Wang F, Jiang BY, Chen SJ, Ren MZ (2019) Surface collapse control under thick unconsolidated layers by backfilling strip mining in coal mines. Int J Rock Mech Min Sci 113:268–277

Wu N, Liang ZZ, Zhou JR, Zhang YZ (2020) Energy evolution characteristics of coal specimens with preformed holes under uniaxial compression. Geomech Eng 20(1):55–66

Yang JH, Lu WB, Jiang QH, Yao C, Jiang SH, Tian L (2016) A study on the vibration frequency of blasting excavation in highly stressed rock masses. Rock Mech Rock Eng 49(7):2825–2843

Yin DW, Chen SJ, Liu XQ, Ma HF (2018) Effect of joint angle in coal on failure mechanical behaviour of roof rock–coal combined body. Q J Eng Geol Hydrogeol 51(2):202–209

Zhao YX, Jiang YD, Zhu J, Sun GZ (2008) Experimental study on precursory information of deformation of coal-rock composite sample before failure. Chin J Rock Mech Eng 27(2):339–346

Zhao TB, Guo WY, Lu CP, Zhao GM (2016) Failure characteristics of combined coal-rock with different interfacial angles. Geomech Eng 11(3):345–359

Zhang ZT, Liu JF, Wang L, Wang HT, Zuo JP (2012) Effects of combination mode on mechanical properties and failure characteristics of the coal-rock combinations. J China Coal Soc 37(10):1677–1681

Zuo JP, Chen Y, Zhang JW, Wang JT, Sun YJ, Jiang GH (2016) Failure behavior and strength characteristics of coal-rock combined body under different confining pressures. J China Coal Soc 41(11):2706–2713